Synthesis of Nickel Oxide Nanoarchitecture Crystals as an Advanced Electrode Material for Supercapacitors

S. Nelson Amirtharaj[1,2,*,], M. Mariappan[2] and V. Beaula Premavathi[1,]

[1]Department of Chemistry, T.B.M.L. College (Affiliated to Bharathidasan University), Porayar-609307, India
[2]Department of Chemistry, Thiru. Vi. Ka. Government Arts College (Affiliated to Bharathidasan University), Thiruvarur-610003, India

*Corresponding author: E-mail: snelsamir@gmail.com

A NiO nanoarchitecture with a chain-like structure material was synthesized using a CTAB-assisted sonochemical method and then applied as an electrode in supercapacitors. Spectral analysis like XRD, FTIR and SEM was used to characterize the crystalline nature, internal structure and morphological properties of NiO nanoarchitecture. At a scan rate of 5 mV s^{-1}, the NiO material exhibits a pseudo-capacitive charge storage mechanism and provides a specific capacitance of 562 with good rate capabilities. Moreover, the chain-like NiO material exhibits outstanding cycle stability, retaining 96% of the original capacitance after 3,000 cycles at a scan rate of 100 mV s^{-1}. The high-performance, chain-like nanostructured NiO material is easy to make and is of great interest for improved energy storage devices.

Keywords: Sonochemical, CTAB, Chain-like NiO, Supercapacitors, Energy.

INTRODUCTION

The rapid increase in energy consumption and the expanding renewable energy sector have stimulated extensive research endeavors in the field of sophisticated energy storage devices [1]. Due to their accessibility, sustainability and better performance, energy storage such as fuel cells, supercapacitors and batteries, have recently got a lot of attraction in recent days. Among them, pseudocapacitors are attracting considerable interest in electronic vehicles and devices owing to their inherent combined qualities of the high charge density of chemical batteries and the larger rate capability feature of traditional electrical double-layer capacitors. Supercapacitors also have a variety of interesting characteristics, including a long term cycle life, reduced internal resistance, quick charge and discharge rates and a relatively low price [2-4]. Generally, metal oxides and conducting polymers deliver pseudo capacitance behaviour due to their redox nature [5-7]. Interestingly, as compared to EDLC, pseudocapacitors have superior electrochemical features. Consequently, it is vital to create pseudocapacitor materials using inexpensive and ecologically friendly synthetic methods that have good electrochemical properties. Supercapacitor has many potential advantages over the battery. In a supercapacitor, the charge-up time is very low and has wide operating tempera-

tures. It can perform 95% more efficiently than the battery (60-80%). Commonly, carbon-based materials like graphene and carbon nanotubes are suggested electrode materials for diamond-like carbon (DLC) making and for pseudocapacitor transition metal oxide, polypyrrole are recommended materials which are also called conducting polymers [8,9]. The transition metal oxide-mediated pseudocapacitors are most preferred due to their operating lifetime and highest electrical power delivery. In addition, it has a wide range of applications in sensors, photo-catalytic effects, magnetic and electrochemical performances [8].

As supercapacitor electrode materials, several transition metal oxides have been studied of them, ruthenium oxide has received much more interest as an electrode for pseudocapacitors. Due to the high specific capacitance (1580 F g^{-1}) and excellent charge-discharge process along with a boundless electrical conducting properties [10]. However, because of its high toxicity and cost the ruthenium oxide is the main disadvantaged. Due to this framework, it is necessary to prepare low cost new materials and for that the materials such as ZnO [11], MnO$_2$ [12], MoO$_3$ [13], NiO [14], CuO [15], V$_2$O$_5$ [16] and Co$_3$O$_4$ [17] to be demonstrated as probable electrode materials for high performance supercapacitor applications. Among them, NiO is a desirable material for pseudocapacitors, since it has favourable

features such as being inexpensive and environmentally acceptable. Additionally, theoretically at 0.5 V potential it shows high capacitance of 2583 F g^{-1}. Based on the nature and density of defects, NiO belongs to p-type semiconductor metal oxide with a wide bandgap that varies between 3.6 and 4.0 eV [18]. The NiO material is not only utilized in supercapacitors but also used in various fields like batteries [19], fuel cell catalysis [20], dye sensitized solar cells [21] and sensors [22]. Depending on the morphologies, the electrochemical properties of NiO with a nanostructure vary significantly. This is due to the fact that the structural morphologies play a role in determining the velocity of ion migration during the electrochemical process.

There are various techniques have been adopted to produce different morphologies of NiO material (hydrothermal [23], electrospinning [24], solid-state synthesis [25] and electro-deposition method [26]) for supercapacitor applications. Each synthetic approach has its strengths and drawbacks to prepare various NiO morphologies. Among them, the sonochemical approach becomes more advantageous for nanostructured materials development. Till now, various morphologies such as nanorods [27], nanobelts [28], nanoflowers [29] and nano rice [30] have been synthesized using the sonochemical method.

In this endeavor, the chain-like NiO materials were synthesized using a CTAB-assisted sonochemical technique, after that by a subsequent calcination process. Furthermore, CTAB has been used as a template to alter the surface properties of NiO in order to create unique morphologies in the material. The basic properties such as crystalline behaviour, nodding nature and morphologies were demonstrated by various analytical techniques. The CV and GCD studies were used for examine the supercapacitor properties of the synthesized NiO materials. In addition, the method of synthesis is simple and economical to carry out.

EXPERIMENTAL

From SRL (India), nickel nitrate hexahydrate (Ni(NO$_3$)$_2$· 6H$_2$O) as well as ethanol and cetyltrimethylammonium bromide (CTAB) were purchased. N-Methyl-2-pyrrolidone (NMP), carbon black and polyvinylidene difluoride (PVDF) were purchased from Sigma-Aldrich, India. Stainless steel foil, KOH and NaOH were procured from Alfa aeser. Without additional purification, all the reagents were also used as supplied and throughout the experiment, deionized water was used.

Synthesis of NiO materials: A typical step of synthesis, dissolved 0.5 M of Ni(NO$_3$)$_2$· 6H$_2$O in 100 mL of deionized water was added to a solution of 0.01 M of CTAB dissolved in 100 mL of diisopropyl iodide. After that, the precursor solution for nickel nitrate was gradually mixed into the solution for CTAB while continuing to stirred the mixture for an additional 0.5 h to obtain a homogenous solution. To get the precipitate, 10 mL of 2 M NaOH was mixed to this precursor solution. After that, the solution was put into an ultrasonic bath so that it could be irradiated with ultrasound. The final products were then centrifuged and washed with ethanol and water, respectively. After being thoroughly ground with a mortar and pestle, the washed material was dried at 70 ºC for 12 h in a hot air oven. The final product was calcined at 300 ºC for 3 h and then the

ultrasound irradiation time was varied to 0, 20 and 40 min to get the NiO-1, NiO-2 and NiO-3 materials.

Characterization and electrode preparation for supercapacitor analysis: The BRUKER D8 Advance equipment with Cu*K*α radiation (λ = 0.154060 nm) operated at 45 kV, 40 mA and a scanning speed of 2º/min was used to record the X-ray diffraction (XRD) data. The SHIMADZU model IR Affinity 1 instrument, which has a wavelength range of 4000 to 400 cm^{-1}, was used to record the Fourier transform spectroscopic analysis (FTIR) studies. A high-resolution scanning electron microscopy was used to analyze the surface structural characteristics (F E I Quanta FEG 200 instrument). Utilizing a biological instrument (model SP-151) with three electrodes– a working electrode made of stainless-steel foil covered with active materials, a reference electrode made of saturated calomel and a counter electrode made of platinum foil. For electrochemical investigations, acetylene black, poly(vinylidene fluoride) and active material were mixed in a ratio of 80:10:10 in N-methyl-2-pyrrolidone (NMP)to obtain a slurry, which was then used to prepare the active electrode. The doctor blade procedure was used to evenly coat the resulting slurry on the stainless steel foil and dried for 12 h at 70 ºC in a vacuum oven. The properties of the supercapacitor were assessed using the dried electrodes and the material weight of the working electrode was around 3.5 mg.

RESULTS AND DISCUSSION

XRD studies: XRD was used to analyze the crystallinity and purity of produced NiO materials such as NiO-1, NiO-2 and NiO-3. All of the diffraction peaks demonstrate extremely low intensity and a broad nature, confirming that the synthesized NiO materials include nanoparticles of tiny size (Fig. 1). The peaks at 2θ = 37.30º, 43.5 º, 62.23º, 75.21º and 79.23º are related with the crystalline planes of 111, 200, 220, 311 and 222, respectively. The diffraction peaks of NiO materials confirmed the establishment of the face-centred cubic (FCC) crystalline structure of NiO materials, which has been indexed the JCPDS card number 04-0835. All of the XRD patterns revealed that the materials include only FCC cubic NiO material and no
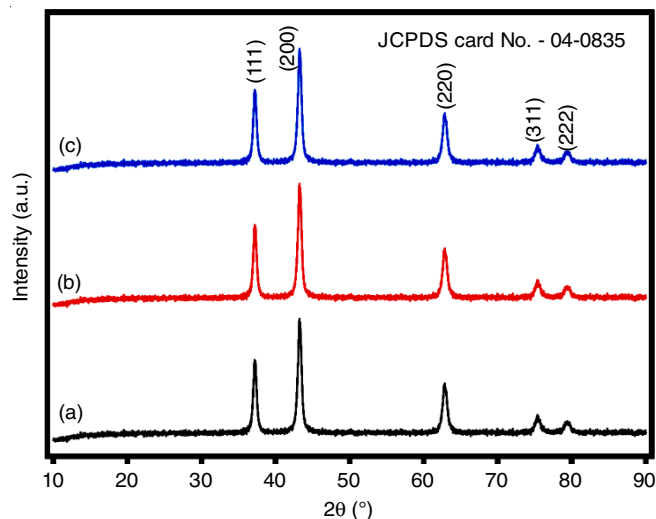

Fig. 1. XRD analysis of (a) NiO-1; (b) NiO-2 and (c) NiO-3 samples

impurities were detected, confirming that the high purity of the materials was attained using the CTAB-assisted sono-chemical technique.

FTIR studies: FTIR spectral studies were done to evaluate the internal properties and bonding features of NiO materials as shown in Fig. 2. Three distinctive peaks have appeared at 414, 571 and 1034 cm^{-1} in NiO materials. The peak at 414 cm^{-1} is due to the stretching vibration of Ni-O bond in the NiO material, whereas the peak at 571 cm^{-1} is due to the bending vibration of Ni with hydroxide entities. The peak at 1034 cm^{-1} is attributed to the distinctive stretching vibration of SO_4 molecules that originated from CTAB template [31]. The XRD and FTIR analyses confirmed the formation of NiO materials using a CTAB-assisted sonochemical synthesis.
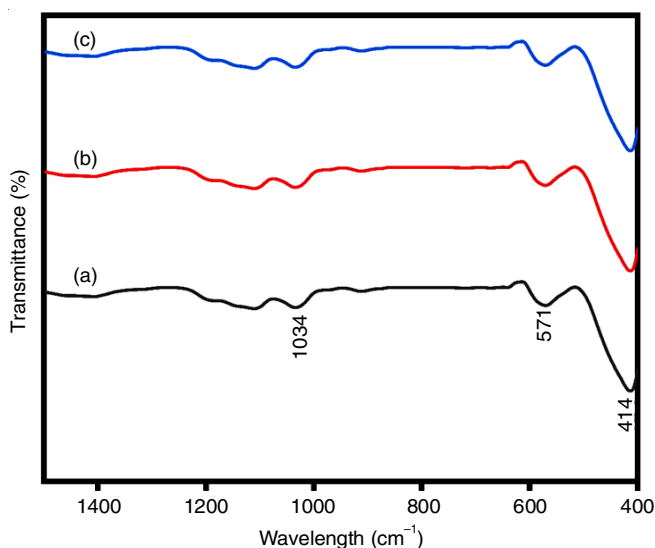

Fig. 2. FTIR analysis of (a) NiO-1; (b) NiO-2 and (c) NiO-3 samples

Morphological analysis: As illustrated in Fig. 3, the morphology of the prepared NiO materials was analyzed by HR-SEM. Fig. 3a-b show the lower and higher magnification SEM images of NiO-1 material synthesized. TThese findings support the hypothesis that the morphological characteristics of NiO materials are more strongly influenced by the CTAB template and ultrasonic irradiation period than by the CTAB template alone. With an average size of 120 ± 10 nm, a granular form is clearly visible in the SEM image moreover, small nanoparticles of 10 nm in size are also visible in SEM images. When the period of ultrasonic irradiation is increased to 20 min (NiO-2), chain-like NiO structures emerge, as seen in Fig. 3c-d. It is evident that the tiny granular-shaped nanoparticles combine in a specific manner and form chain-like structures. The cavities also formed between the chain, which are very useful for supercapacitor application. The size and particles of the chains getting increased when the ultrasound irradiation time increased to 40 min (NiO-3) as shown in Fig. 3e-f. In addition, the agglomeration of particles also getting increased. The findings of this study provide evidence that both the CTAB template and ultrasonic irradiation time exert a significant impact on the morphological characteristics of NiO materials.

Electrochemical studies: Using a three-electrode electrochemical setup, the electrochemical properties of NiO materials were analyzed. Using standard CV and GCD techniques in a 1 M KOH electrolyte, the electrochemical properties were tested. Fig. 4a-c displays the CV curves for NiO materials. In addition, it exhibits redox peaks, indicating that the specific capacitance of the materials is primarily related to the Faradaic pseudocapacitor charge storage mechanism and that the electron transfer is reversible. The anodic peak corresponds to the transformation of NiO to NiOOH in alkaline electrolytes, whereas the cathodic peak corresponds to the reverse reaction. According
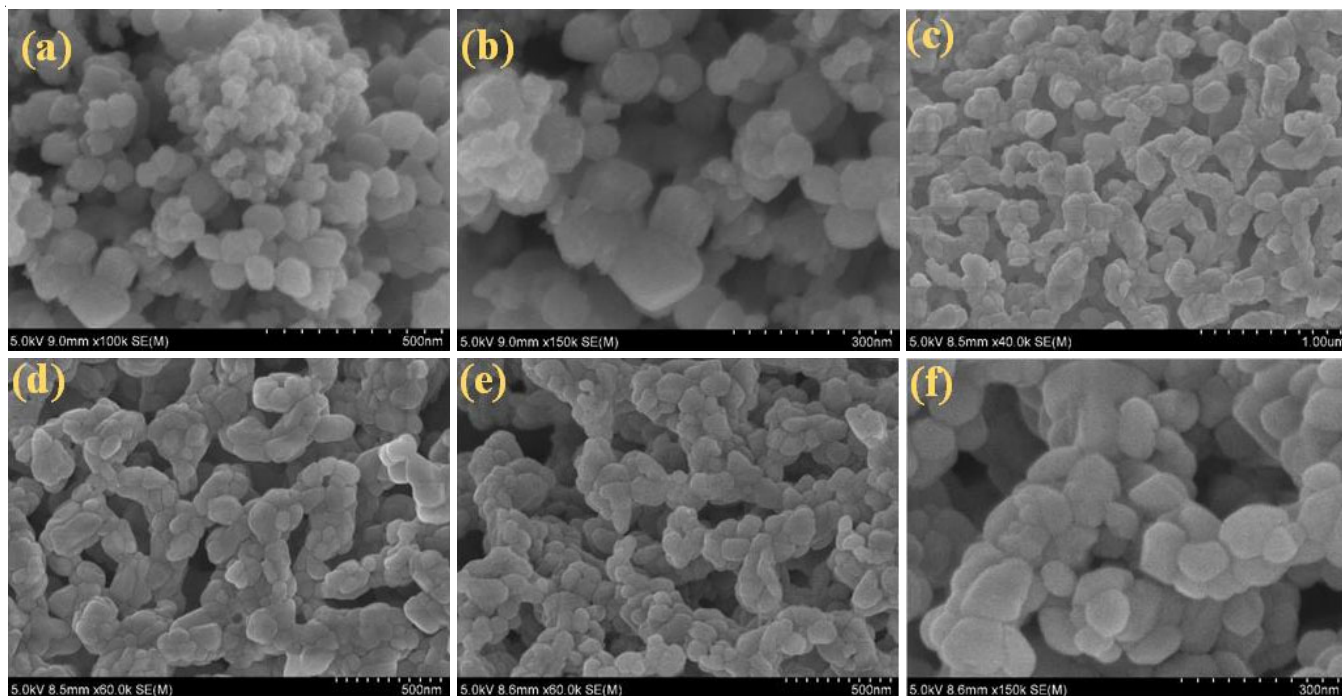

Fig. 3. HR-SEM images (a) & (b) NiO-1; (c) & (d) NiO-2 and (e) & (f) NiO-3 materials
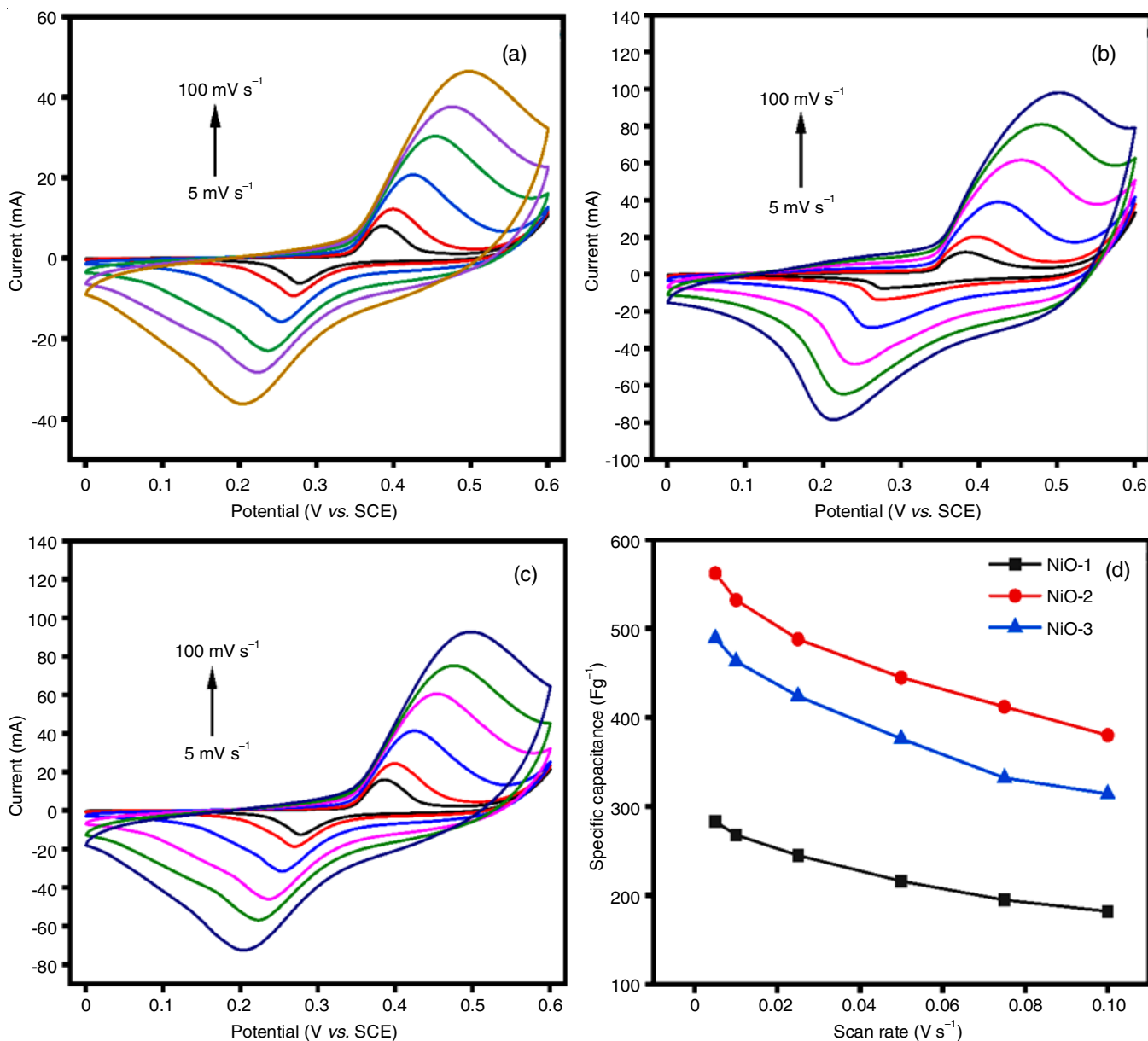
Fig. 4. Cyclic voltammograms of (a) NiO-1; (b) NiO-2, (c) NiO-3 materials and specific capacitance *vs.* scan rate graph

to the following eqn. 1, these anodic and cathodic peaks demonstrate the transition of oxidation states in NiO [32].

$$NiO + OH^- \rightleftharpoons NiOOH + e^- \quad (1)$$

When the scan rate is increased from 5 to 100 mV s^{-1}, the shape profiles of the CV curves do not change much, indicating that the electrode material has great electrochemical reactivity and rapid activation, indicating that it has a high electrical conductivity. The value of redox potentials moves in more positive and negative positions as the sweep rate increase. This is because to the stronger electric polarization and the irreversible reactions that take place at a faster scan rate [33]. Even during the electrochemical reaction process, electronic neutralization will not be met since the rate of ion diffusion during the electrochemical analysis restricts this redox reaction [34]. The area under the CV curves is directly proportional to the specific capacitance of the electrode materials NiO-2 had the

highest area under the CV curve of all of the NiO electrodes, which is confirmation of its excellent behaviour as a supercapacitor. Eqn. 2 is used to calculate the specific capacitance of the curves.

$$Cs = \frac{\int idv}{2 \times S \times M \times V} \quad (2)$$

where Cs is the specific capacitance in Fg^{-1}, M is the active mass (g), $\int idV$ is the integrated area, S is the scan rate (mV s^{-1}) and V is the voltage window (V). The NiO-1, NiO-2 and NiO-2 had the highest area under the CV curve of all of the NiO electrodes, which is confirmation of its excellence as a supercapacitor. The NiO-1, NiO-2, NiO-3 electrodes are delivered the specific capacitance of 283, 489 and 562 F g^{-1}, respectively at a scan rate of 5 mV s^{-1}. It is fascinating to observe that the specific capacitance of the electrodes made of NiO-2 materials is greater than that of NiO-1 and NiO-3 electrode materials.

The NiO-3 nanoparticles deliver a lower capacitance than NiO-2, which is due to a more aggregated structure. The specific capacitance is reduced by this type of structure, which prevents electrolyte ions from penetrating the inner side of materials. The graph of scan rate *vs.* specific capacitance, as represented in Fig. 4d, was used to analyze the rate capability of the NiO materials. It demonstrated that when the scan rate rises, the specific capacitance drops. The ion-exchange process can explain the decrease in specific capacitance. The OH⁻ ions get adequate time to diffuse into the NiO materials when the scan rate is low, but they have significantly less time to get close to the electrode material when the scan rate is high [35].

Galvanostatic charge-discharge (GCD) studies: GCD studies were carried out in 1 M KOH solution with a platinum foil serving as the counter electrode and a saturated calomel electrode serving as the reference electrode to further analyze the electrochemical properties and applicability of chain-like NiO nanoparticles such as NiO-1, NiO-2 and NiO-3 are shown in Fig. 5a-c. All of the charge-discharge curves exhibit the non-linear behaviour and this behaviour changes with the profile of the EDLC mechanism, confirming that the charge storage behaviour is that of a pseudocapacitance. This pattern is comparable with the cyclic voltammetry analysis. The NiO materials' superior pseudocapacitive behaviour is confirmed by the lower iR drop. Among all the electrodes, NiO-2 delivers a higher discharge time than NiO-1 and NiO-3 materials, confirming the excellent supercapacitor behaviour of the NiO-2 materials. The specific capacitance may be derived from the GCD curves using eqn. 3:

$$Cs = \frac{I\Delta t}{m\Delta V} \quad (3)$$

where I is the input current density (Ag^{-1}), Δt is the discharge time (s) in the GCD curves, m is the weight of active electrode material and ΔV is the potential window. At a current density of 1 A g⁻¹, the NiO electrodes NiO-1, NiO-2 and NiO-3 provide specific capacitances of 282, 448 and 520 F g⁻¹, respectively. The specific capacitance *vs.* current density graph of all the prepared NiO electrodes is shown in Fig. 5d.

When the current density is increased from 1 to 30 A g⁻¹, the specific capacitance values rapidly decrease. Similar to the capacitance fluctuation trend seen in CV studies, the specific
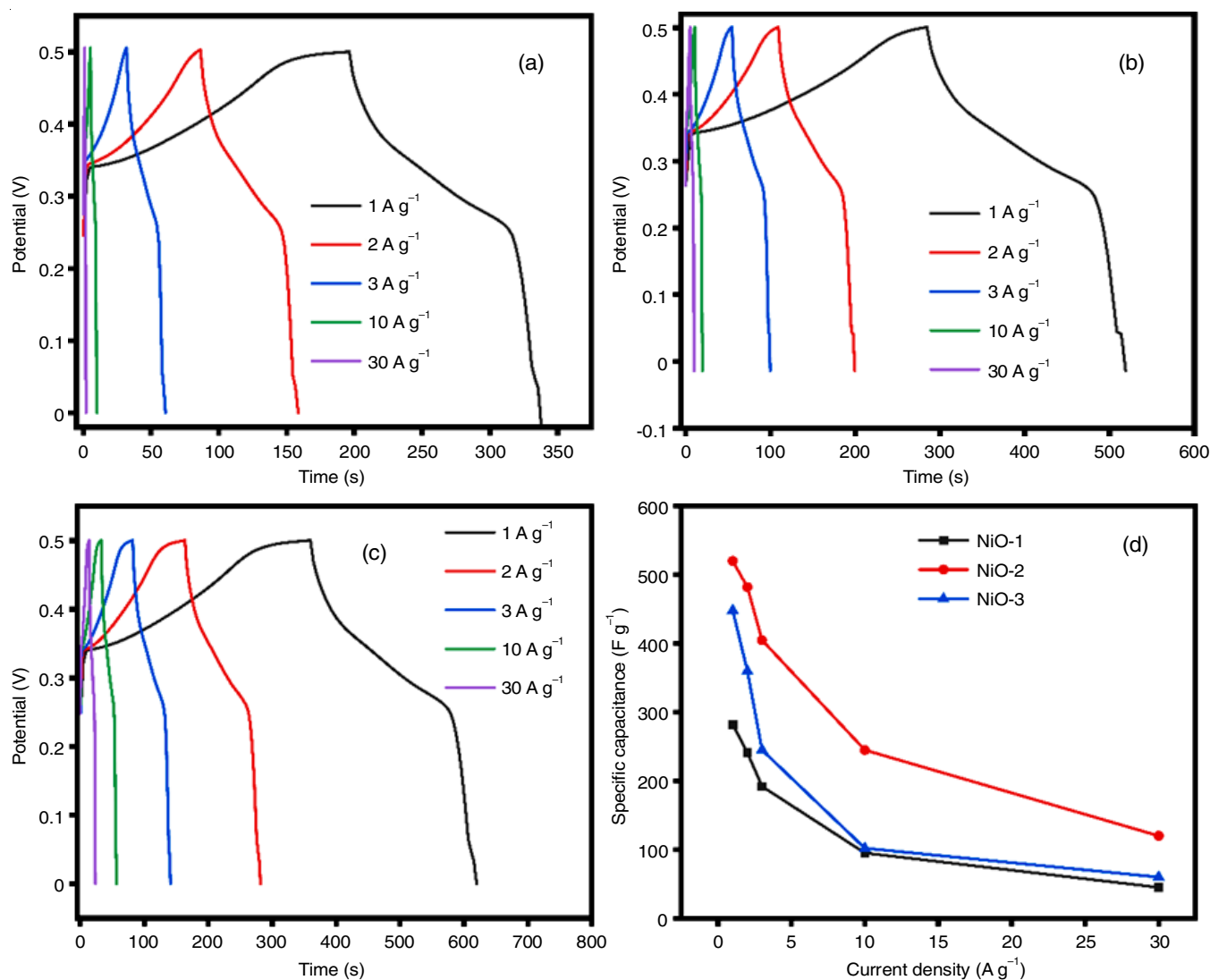

Fig. 5. GCD analysis of (a) NiO-1; (b) NiO-2, (c) NiO-3 materials and specific capacitance *vs.* current density graph

capacitance declines as the discharge current rises. For applications using supercapacitors, the energy and power density parameters of the electrode materials are crucial. Power and energy densities are calculated using eqns. 4 and 5 and the resultant Regone plot is shown in Fig. 6.

$$E = \frac{1}{2} \frac{C \times V^2}{3.6} \quad (4)$$

$$P = \frac{E \times 3600}{t} \quad (5)$$

where E is energy density (Wh Kg^{-1}), C is the specific capacitance from GCD curves (F g^{-1}), V potential window (V), P is the power density (W Kg^{-1}) and t is the discharge time (in seconds). The energy densities of NiO-1, NiO-2 and NiO-3 electrodes were 9.7, 18 and 15.5 Wh Kg^{-1}, respectively, at a current density of 1 Ag^{-1}, whereas they exhibit power densities were 3600, 5400 and 4555 W Kg^{-1}. In this study, the long-term cyclic stability of the NiO electrodes was examined by repeatedly performing the CV analysis for 3000 cycles at a scan rate of 100 mV s^{-1}, as shown in Fig. 7a.
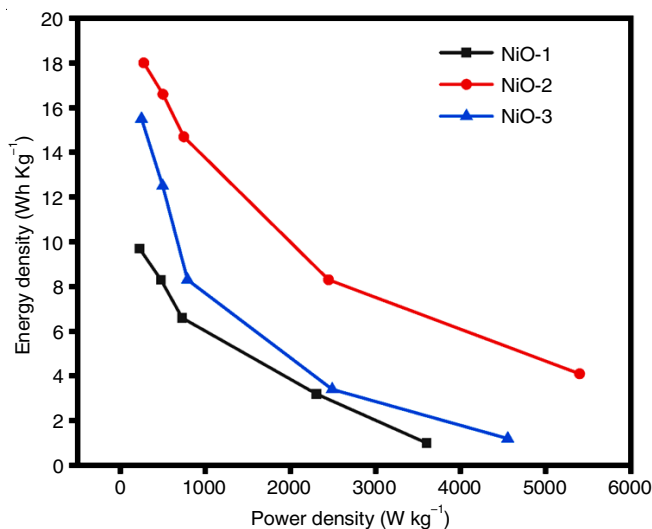

Fig. 6. Ragone plot of NiO materials

In addition, the 1st cycle and the 3000th cycle of the cyclic stability assessments of the NiO-1, NiO-2 and NiO-3 electrodes are shown in Fig. 7b-d, respectively. It is clear that the specific
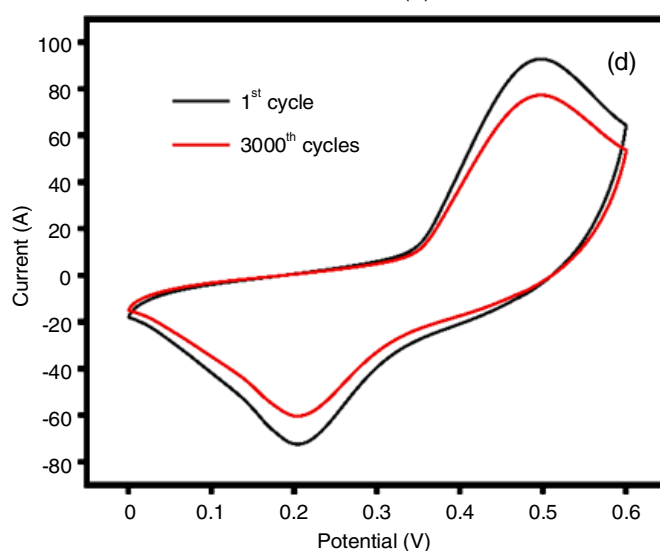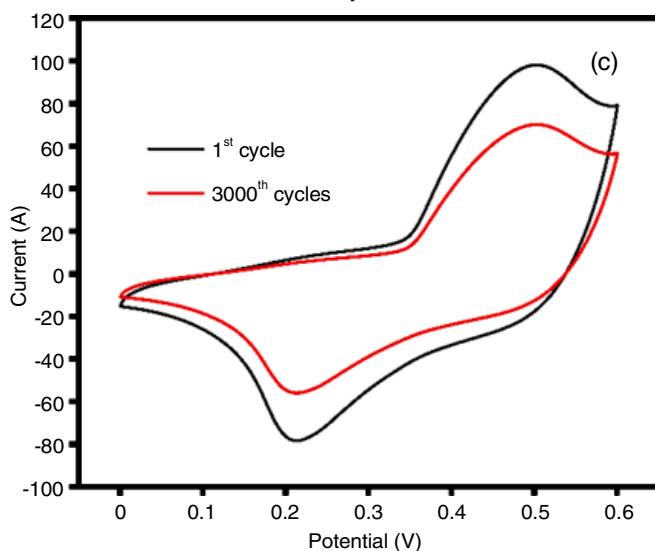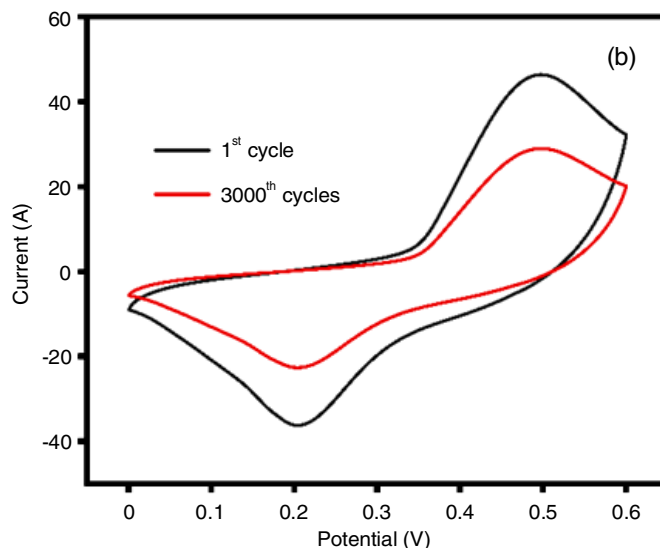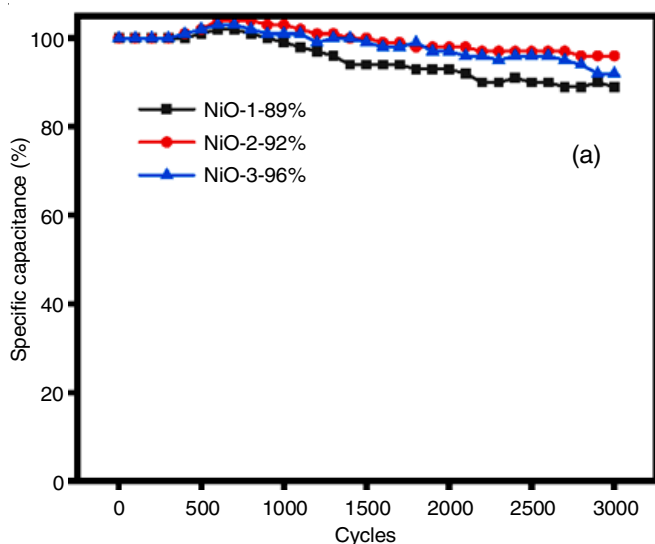

Fig. 7. (a) Cycle life test of NiO materials at a scan rate of 100 mV s^{-1}. 1st and 3000th CV curves of (a) NiO-1; (b) NiO-2 and (c) NiO-3 materials

capacitance retention of NiO electrodes steadily increases at initial cycles, then declines slowly. This signifies that the electrode is being activated during initial cycles of cyclic stability analysis [36]. The overall initial capacitance loss for NiO-1, NiO-2 and NiO-3 electrodes were 11%, 4% and 8%, respectively. Among all the electrodes, a chain-like NiO material (NiO-2) demonstrates the superior cyclic stability performance with 96% of initial specific capacitance retention and exhibits an outstanding supercapacitor characteristics with excellent specific capacitance and good long-term cyclic stability when examined as a supercapacitor electrode material.

Conclusion

In summary, a simple, economical synthetic approach has been adopted for the synthesis of NiO nanostructures for supercapacitor electrode applications. The ultrasound irradiation and CTAB template are the two significant parameters to generate the chain-like NiO nanoarchitecture. The chain-like NiO nanostructure not just renders a large surface area in addition, gives a pathway for continuous electron transport route for electrolyte ion throughout the electrochemical process. As prophesized, the resultant chain-like NiO structure (NiO-2) exhibited a high specific capacitance of 562 F g^{-1} at a scan rate of 5 mV s^{-1}, together with outstanding rate capability and cyclic stability, confirming its suitability for supercapacitor device application.

CONFLICT OF INTEREST

The authors declare that there is no conflict of interests regarding the publication of this article.

REFERENCES

1. H. Peng, G. Ma, J. Mu, K. Sun and Z. Lei, *J. Mater. Chem. A Mater. Energy Sustain.*, **2**, 10384 (2014); https://doi.org/10.1039/C4TA01899K

2. S. Amaresh, K. Karthikeyan, I.C. Jang and Y.S. Lee, *J. Mater. Chem. A Mater. Energy Sustain.*, **2**, 11099 (2014); https://doi.org/10.1039/C4TA01633E

3. W. Chen, R.B. Rakhi, M.N. Hedhili and H.N. Alshareef, *J. Mater. Chem. A Mater. Energy Sustain.*, **2**, 5236 (2014); https://doi.org/10.1039/c3ta15245f

4. R. Wang, X. Yan, J. Lang, Z. Zheng and P. Zhang, *J. Mater. Chem. A Mater. Energy Sustain.*, **2**, 12724 (2014); https://doi.org/10.1039/C4TA01296H

5. T. Pettong, P. Iamprasertkun, A. Krittayavathananon, P. Sirisinudomkit, P. Sukha, A. Seubsai, M. Chareonpanich, P. Kongkachuichay, J. Limtrakul and M. Sawangphruk, *ACS Appl. Mater. Interfaces*, **8**, 34045 (2016); https://doi.org/10.1021/acsami.6b09440

6. A.V. Radhamani, K.M. Shareef and M.S.R. Rao, *ACS Appl. Mater. Interfaces*, **8**, 30531 (2016); https://doi.org/10.1021/acsami.6b08082

7. J.S. Chen, C. Guan, Y. Gui and D.J. Blackwood, *ACS Appl. Mater. Interfaces*, **9**, 496 (2017); https://doi.org/10.1021/acsami.6b14746

8. P. Forouzandeh, V. Kumaravel and S.C. Pillai, *Catalysts*, **10**, 969 (2020); https://doi.org/10.3390/catal10090969

9. S. Bose, T. Kuila, A.K. Mishra, R. Rajasekar, N.H. Kim and J.H. Lee, *J. Mater. Chem.*, **22**, 767 (2012); https://doi.org/10.1039/C1JM14468E

10. C.C. Hu, K.H. Chang, M.C. Lin and Y.T. Wu, *Nano Lett.*, **6**, 2690 (2006); https://doi.org/10.1021/nl061576a

11. Q. Luo, P. Xu, Y. Qiu, Z. Cheng, X. Chang and H. Fan, *Mater. Lett.*, **198**, 192 (2017); https://doi.org/10.1016/j.matlet.2017.04.032

12. S. Zhao, T. Liu, D. Hou, W. Zeng, B. Miao, S. Hussain, X. Peng and M.S. Javed, *Appl. Surf. Sci.*, **356**, 259 (2015); https://doi.org/10.1016/j.apsusc.2015.08.037

13. J. Li and X. Liu, *Mater. Lett.*, **112**, 39 (2013); https://doi.org/10.1016/j.matlet.2013.08.094

14. F.I. Dar, K.R. Moonoosawmy and M. Es-Souni, *Nanoscale Res. Lett.*, **8**, 363 (2013); https://doi.org/10.1186/1556-276X-8-363

15. S.K. Shinde, H.M. Yadav, G.S. Ghodake, A.A. Kadam, V.S. Kumbhar, J. Yang, K. Hwang, A.D. Jagadale, S. Kumar and D.Y. Kim, *Colloids Surf. B Biointerfaces*, **181**, 1004 (2019); https://doi.org/10.1016/j.colsurfb.2019.05.079

16. J. Yang, T. Lan, J. Liu, Y. Song and M. Wei, *Electrochim. Acta*, **105**, 489 (2013); https://doi.org/10.1016/j.electacta.2013.05.023

17. X.H. Xia, J.P. Tu, Y.J. Mai, X. Wang, C. Gu and X. Zhao, *J. Mater. Chem.*, **21**, 9319 (2011); https://doi.org/10.1039/c1jm10946d

18. H. Wang, H. Yi, X. Chen and X. Wang, *Electrochim. Acta*, **105**, 353 (2013); https://doi.org/10.1016/j.electacta.2013.05.031

19. X. Wang, Z. Yang, X. Sun, X. Li, D. Wang, P. Wang and D. He, *J. Mater. Chem.*, **21**, 9988 (2011); https://doi.org/10.1039/c1jm11490e

20. K. Czelej, K. Cwieka, J.C. Colmenares and K.J. Kurzydlowski, *Appl. Catal. B*, **222**, 73 (2018); https://doi.org/10.1016/j.apcatb.2017.10.003

21. N. Li, E.A. Gibson, P. Qin, G. Boschloo, M. Gorlov, A. Hagfeldt and L. Sun, *Adv. Mater.*, **22**, 1759 (2010); https://doi.org/10.1002/adma.200903151

22. I. Hotový, J. Huran, L. Spiess, R. Capkovic and Š. Hašcik, *Vacuum*, **58**, 300 (2000); https://doi.org/10.1016/S0042-207X(00)00182-2

23. P. Justin, S.K. Meher and G.R. Rao, *J. Phys. Chem. C*, **114**, 5203 (2010); https://doi.org/10.1021/jp9097155

24. S. Liu, J. Jia, J. Wang, S. Liu, X. Wang, H. Song and X. Hu, *J. Magn. Magn. Mater.*, **324**, 2070 (2012); https://doi.org/10.1016/j.jmmm.2012.02.017

25. M. Salavati-Niasari, F. Mohandes, M. Mazaheri, F. Davar, M. Monemzadeh and N. Yavarinia, *Inorg. Chim. Acta*, **362**, 3691 (2009); https://doi.org/10.1016/j.ica.2009.04.025

26. M.S. Wu, Y.A. Huang, C.H. Yang and J.J. Jow, *Int. J. Hydrogen Energy*, **32**, 4153 (2007); https://doi.org/10.1016/j.ijhydene.2007.06.001

27. G. Kianpour, M. Salavati-Niasari and H. Emadi, *Ultrason. Sonochem.*, **20**, 418 (2013); https://doi.org/10.1016/j.ultsonch.2012.08.012

28. Y.J. Chen, F.N. Meng, H.L. Yu, C. Zhu, T. Wang, P. Gao and Q. Ouyang, *Sens. Actuators B Chem.*, **176**, 15 (2013); https://doi.org/10.1016/j.snb.2012.08.007

29. C. Qi, Y.J. Zhu, C.T. Wu, T.-W. Sun, Y.-Y. Jiang, Y.-G. Zhang, J. Wu and F. Chen, *RSC Adv.*, **6**, 9686 (2016); https://doi.org/10.1039/C5RA26231C

30. M. Zhang, A. Zhao, D. Li, H. Sun, D. Wang, H. Guo, Q. Gao, Z. Gan and W. Tao, *Analyst*, **137**, 4584 (2012); https://doi.org/10.1039/c2an35758e

31. H.M. Mohaideen, S.S. Fareed and B. Natarajan, *Surf. Rev. Lett.*, **26**, 1950043 (2019); https://doi.org/10.1142/S0218625X19500434

32. Y. Zeng, L. Wang, Z. Wang, J. Xiao and H. Wang, *Mater. Today Commun.*, **5**, 70 (2015); https://doi.org/10.1016/j.mtcomm.2015.11.001

33. F. Chen, W. Zhou, H. Yao, P. Fan, J. Yang, Z. Fei and M. Zhong, *Green Chem.*, **15**, 3057 (2013); https://doi.org/10.1039/c3gc41080c

34. L. Fan, L. Tang, H. Gong, Z. Yao and R. Guo, *J. Mater. Chem.*, **22**, 16376 (2012); https://doi.org/10.1039/c2jm32241b

35. J. Yesuraj and S.A. Suthanthiraraj, *J. Mol. Struct.*, **1181**, 131 (2019); https://doi.org/10.1016/j.molstruc.2018.12.087

36. J. Yesuraj, S. Austin Suthanthiraraj and O. Padmaraj, *Mater. Sci. Semicond. Process.*, **90**, 225 (2019); https://doi.org/10.1016/j.mssp.2018.10.030